

Preliminary understanding of initial reaction process for subbituminous coal pyrolysis with molecular dynamics simulation



Jin-Hui Zhan, Rongcheng Wu, Xiaoxing Liu, Shiqiu Gao, Guangwen Xu*

State Key Laboratory of Multiphase Complex Systems, Institute of Process Engineering, Chinese Academy of Sciences, Beijing 100190, PR China

HIGHLIGHTS

- Subbituminous coal pyrolysis was investigated using ReaxFF molecular dynamics.
- Primary decomposition reactions begin with intramolecular bond cleavage.
- The formation mechanisms for typical pyrolysis products were explored.
- Phenoxy groups play a key role in the hydrogen transfer process of gas generation.
- The reaction mechanisms are coincident with previous experimental results.

ARTICLE INFO

Article history:

Received 23 January 2014

Received in revised form 19 May 2014

Accepted 1 June 2014

Available online 14 June 2014

Keywords:

Subbituminous coal

Pyrolysis

Reactive molecular dynamics

Reaction mechanism

ABSTRACT

A series of molecular dynamics simulations using the ReaxFF reactive force field was carried out to investigate the mechanism of initial thermal decomposition associated with pyrolysis of a kind of subbituminous coal. The calculation results show that the primary decomposition reactions of Hatcher subbituminous model begin with intramolecular changes such as the cleavage of unstable C–C and C–O bonds. The formation mechanisms for typical pyrolysis products were explored. For example, the initial pathway for the formation of CO is by the decarbonylation of carbonyl or carboxyl group, while CO₂ is mainly produced by hydrogen transfer and decarboxylation of carboxyl groups. CH₄ can be formed mainly by CH₃ free radical abstracting a hydrogen atom from the hydroxyl group. H₂ is formed by two hydrogen atoms from one or two groups bonding together, which makes the residue fragments more stable. Hydrogen can also react with oxygen-containing free radicals or unsaturated bonds. Combining ReaxFF molecular dynamics (RMD) simulation and density functional theory (DFT) calculation, we find that the free radical C₉H₉O· is an important fragment during the pyrolysis process of Hatcher subbituminous model. As a precursor for cresol, it can capture hydrogen radical to form intermediate C₉H₁₀O and may continue to produce *o*-cresol and ethylene in the presence of hydrogen resource. These simulation results for the initial pyrolysis process and the reaction mechanisms agree with previous experimental observations.

© 2014 Elsevier Ltd. All rights reserved.

1. Introduction

Subbituminous coal, a type of coal between lignite and bituminous [1], is rich in volatile and has weak caking propensity so that it is highly suitable for pyrolysis to co-produce liquid (tar), gas and solid (char) products. Therefore, there are a lot of technical development works worldwide for establishing the processes of coal pyrolysis [2–6]. However, these technical activities are still seriously suffering from the excessive formation of heavy tar components which tend to cause operational problems in pyrolysis and

also lower the liquid product quality. The solution to this problem is the control of pyrolysis reactions, requiring the clear understanding of the reaction process involved in pyrolysis.

Studies on the mechanism of coal pyrolysis have attracted much attention in the past several decades [7,8]. Meanwhile, knowledge of coal structure has been made significant progress and there are more than 130 coal models proposed since 1940s [9]. The different origin and different degrees of coalification result in structural diversity of coal, especially for the carbon backbone. Several models were published as an aide to understanding the pyrolysis behavior of different rank coal, such as lignite by Tromp and Moulijn [10], bituminous coal by Solomon et al. [11–13]. Structural fragments were collected by destructive techniques

* Corresponding author. Tel.: +86 10 82544886; fax: +86 10 82629912.

E-mail address: gwxu@ipe.ac.cn (G. Xu).

such as flash-pyrolysis or wet chemistry approaches that imposed necessary limitations on the component molecules. The functional groups and their changes during pyrolysis have been measured through experimental approaches, such as FTIR [14,15], NMR [16,17] and GC-MS [18,19], and the structures including heteroatoms, like sulfur [20,21], nitrogen [22,23] and oxygen [24], have been elucidated by X-ray absorption near edge structure (XANES) spectroscopy. However, except *in situ* IR for the detection of changes in the functional groups [14], there is almost no adequate online detection method to obtain more useful information for the continuous variation of species in the process of coal pyrolysis. In addition, coal pyrolysis is also a complex process involving a large number of chemical reactions. These chemical reactions are coupled together, with vast free radical intermediates generated in the initial stage. Such radicals are short-lived species so that they are hard to be captured by traditional experimental approaches. Instead, the computational method should be capable of modeling the chemical reactions involved in coal pyrolysis.

Since the reactive force field (ReaxFF) was developed by van Duin and Goddard et al. [25–27], the computational capabilities for chemical reactions of large systems have been significantly improved. The ReaxFF reactive force field is a general bond order dependent potential. It has been proven to be a smooth transition from non-bonded to bonded interactions and has been demonstrated not only to retain nearly the accuracy of quantum chemistry calculations but also to be as low as classical molecular dynamics at the computational cost. The method has been successfully used to explore the combustion process of lignite and char [28–30], as well as the mechanism of coal pyrolysis [31–35]. For the utility of ReaxFF MD simulation on coal pyrolysis, Salmon et al. [31] investigated early maturation processes in Morwell brown coal [36] with several functional models and a macromolecule, respectively. The macromolecule includes many oxygenic groups, such as methoxyl, hydroxyl and carboxyl groups. The simulation reproduced the defunctionalization process of aromatic side chains in their offline experimental results [36] and showed carbon dioxide as the first product formed. The effects of supercritical solvents (methanol and water) on coal pyrolysis were investigated by Chen et al. [32] using a unimolecular model compound and by Zhang et al. [33] using Wiser [37] bituminous coal model. Their results showed that the solvent decomposed firstly to form active radicals, which attacked to weak bonds leading to the decomposition of coal macromolecular structure. More recently, Zheng et al. [34,35] reported ReaxFF molecular dynamics simulations of bituminous coal pyrolysis using mixed models with Wiser [37], Shinn [38] models and other small molecules to investigate the nascent decomposition processes and product profiles. The sequence of gas generation, the evolution of naphthalene series compounds and the reactions involving CH_3 and OH^- were investigated to understand the pyrolysis behavior. These works give us a useful insight for investigating the mechanism of coal pyrolysis, but in order to control the pyrolysis process and call for high-quality gas and tar products, more microscopic details of chemical reactions during coal pyrolysis, especially for the generation process of key gas (CH_4 , H_2 , CO , and CO_2) and liquid products (phenols) as well as their intermediates, still need to be further explored. Moreover, coal type is an important factor which affects the product distribution of pyrolysis, comparing with the structural feature of lignite and bituminous coal, subbituminous coal contains less ester and side chain than that for lignite, and less aromatic rings than that for bituminous coal.

China has a wealth of subbituminous coal resources, accounting for about one-third of total coal reserves. Recently, we reported a pyrolysis technology to improve the quality of tar using a fixed-bed pyrolyzer enhanced with internals for a weak caking subbituminous coal [39]. In the present work, to achieve the control of

pyrolysis process at the atomic/molecular level, we implemented a series of ReaxFF molecular dynamics (RMD) simulations to investigate the initiation reaction pathways leading to the thermal breakdown of subbituminous coal and describe the formation processes of gas and liquid products. Hatcher [40] subbituminous coal model was selected for studying the mechanisms of pyrolysis. It should be noted that the subbituminous model was derived from the coalification of lignin based on ^{13}C NMR and pyrolysis GC-MS, and the features of this model includes aryl ether linkages, alkyl cyclization at 2,4-position of phenol and less side chain than that for lignite [40]. Although there is no heteroatoms N and S involved in this model, it still well represents the skeleton for subbituminous coal. In addition, the formation processes of possible precursors for typical phenolic products were tracked from the RMD trajectories, and key intermediates as well as transition states were found by assistant DFT calculations.

2. Simulation methods

A subbituminous coal model reported by Hatcher and his coworkers [40] was used as an initial model (Fig. 1a). Firstly, the initial model was built using Marvin program [41], and the geometry optimization of the models was carried out using Forcite Module with the Dreiding force field in Materials Studio (MS) package [42]. Then a minimum energy structure was used to initiate a series of molecular mechanics calculations using simulated annealing to generate several unimolecular conformations. The procedure involved 10 annealing cycles from 300 to 1300 K under constant number, volume and temperature conditions (NVT ensemble) and geometry optimizations were carried out after each cycle. The minimum energy structure was used in next ReaxFF reactive molecular dynamics step.

A macromolecule involving six molecular models with 1110 atoms was immersed in a periodic box ($30 \times 30 \times 30 \text{ \AA}^3$) (Fig. 1b). To achieve an appropriate density of subbituminous coal, the density of this initial macromolecular system was adjusted to 0.78 g/cm^3 ($26.0 \times 25.7 \times 26.3 \text{ \AA}^3$) at 300 K by using NPT (constant number, pressure and temperature) ensemble at pressures of 0.2 GPa with a damping constant of 500 fs. Next, we performed 10 ps no-reaction MD simulation at 300 K NVT ensemble to relax this system. Then, heat up simulations from 300 K to 2800 K at rates of 10, 20, 40 and 80 K/ps for the macromodel were performed to determine the onset temperature of thermal decomposition. Finally, ReaxFF reactive molecular dynamics simulations were performed using NVT ensemble for 1 ns with different temperatures at 1000, 1600, 1800, 2000, 2200 and 2400 K, respectively. The velocity Verlet approach was adopted to integrate and update Newton's equation of motion of atoms with a time step of 0.25 fs. A Berendsen thermostat with a 100 fs damping constant was used for temperature control. System configurations were saved with every 0.5 ps and separate molecular fragments were identified by a ReaxFF bond order upon 0.3. The parameters used in the present RMD study were C/H/O ReaxFF force field parameters [43]. The energy conservation was evaluated by the NVE simulations at different temperatures, which is based on the method reported by van Duin et al. [44] (see supplementary material).

Although the time scale is still many magnitudes lower than that usually observed in experiments, the simulation time (1 ns) is longer than that performed in previous works (no more than 250 ps) for coal pyrolysis. The temperature can affect the reaction rate based on the Arrhenius equation, especially for the reaction with higher energy barrier, which will be obviously accelerated in comparison with that with lower energy barrier [45]. Thus, due to the limitation on computational time scale, we chose a much higher temperature instead of experimental temperature

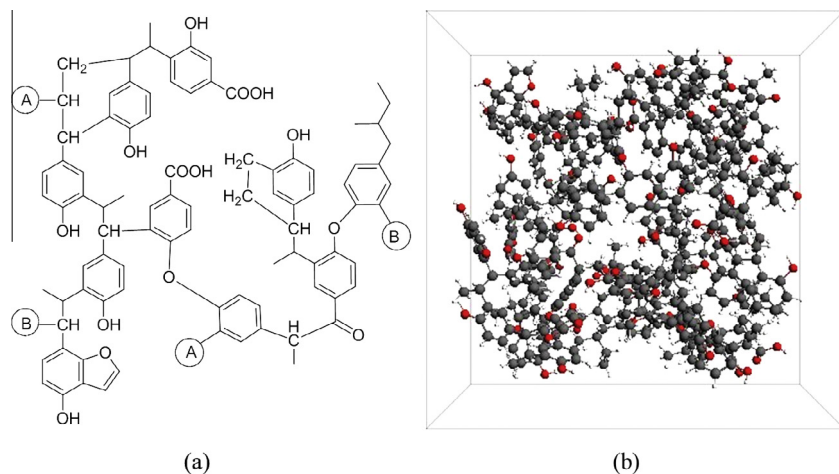


Fig. 1. Structural model for subbituminous coal. (a) 2D unimolecular structure [7], the circled letters indicate connecting sites (e.g. A–A); (b) 3D macromolecule model with six molecules in a periodic box.

to simulate the pyrolysis process of Hatcher subbituminous coal model, which is in the same way as the other pyrolysis studies done by using ReaxFF reactive molecular dynamics.

All ReaxFF reactive molecular dynamics simulations were implemented in ADF software [46]. The DFT calculations were performed by Gaussian03 program [47] using B3LYP hybrid functional [48,49] with 6-31G** basis set for the geometry optimization of the stationary points. The vibrational frequency calculations at the same level were carried out to confirm each stationary point to be either a minimum or transition state (TS). Intrinsic reaction coordinate (IRC) paths were calculated to connect each TS to its corresponding reactant and product. Reported energies include a correction for zero-point energies.

3. Results and discussion

3.1. Initial pyrolysis process of subbituminous coal

Heat up simulations from 300 to 2800 K at rates of 10, 20, 40 and 80 K/ps were performed to determine the onset temperature of thermal decomposition on the picosecond time scale. As shown in Fig. 2, a slow heating rate is beneficial to produce new fragments at low temperature. The new fragment was firstly produced at ~2400 K during the heat up simulation for the rate of 80 K/ps, while it was produced at 1200 K with the heating rate of 10 K/ps. From 1200 K to 2800 K, the slower the heating rate was, the more

the number of new fragments was when reaching the same temperature. It was most probable (three-quarters of the chances) that the initial pyrolysis fragment for various heating rates was the methyl free radical CH_3 , as we can observe from the RMD trajectories. Moreover, methyl radical is a critical precursor of methane, which is an important pyrolysis gas. For the heating rate of 20 K/ps, the methyl free radical was produced at 1930 K. It should also be noted that the initial formation of methyl free radical underwent a series of intra-molecular bond breaking processes, as shown in Fig. 3. This could be ascribed to the intra-molecular unstable tension of Hatcher subbituminous coal model resulting from the substituent and cyclization at 2,4-position of phenol. This structural unit is also present in the lignite model of Morwell coal by Nimz and Salmon et al. [36,50], which is a structural feature for low rank coal. Therefore, intra-molecular C–C bond cleavages occur in succession, and then the free radical rearrangement will happen among C563, C564 and C631, leading to the methyl radical leaving and the formation of a double bond between C563 and C564 (Fig. 3). The methyl radicals, generated by cleavages of C–O bonds of methoxy groups in Salmon et al.'s simulations [31], were not found due to the absence of methoxy groups in Hatcher subbituminous coal [40].

To investigate the kinetics of the thermal decomposition processes, we also performed reactive molecular dynamics simulations using NVT ensemble with 1 ns and the simulation temperature was at 1200, 1600, 1800, 2000, 2200 and 2400 K, respectively, which was chosen based on above heat up simulations. Fig. 4 gives a view of the number of fragments changing with the simulation time under different temperatures. The number of fragments is continuously rising when the temperature is lower than 2000 K. While the temperature is 2400 K, the number of fragments rapidly increases at the beginning of RMD simulation, then decreases at about 600 ps, and finally increases to 98 at 1 ns. The decreases of the number of fragments suggest that some polymerization reactions occur within the corresponding simulation time.

After further analysis of the product compounds observed within the 1 ns RMD simulation at different temperatures, the evolution of product classes with temperature is obtained and displayed in Fig. 5. The number of small fragments (C_1 – C_4 and non-aliphatic gases) increased with elevating temperature, while the number of light tar fragments (C_5 – C_{15} compounds) increased firstly and then kept being stable. The number of heavy tar fragments (C_{16} – C_{40} compounds) decreased when the temperature exceeded 2000 K. The fragments of C_5 – C_{40} are considered as tar in this paper, as well as shown in literatures [16,34], which is based

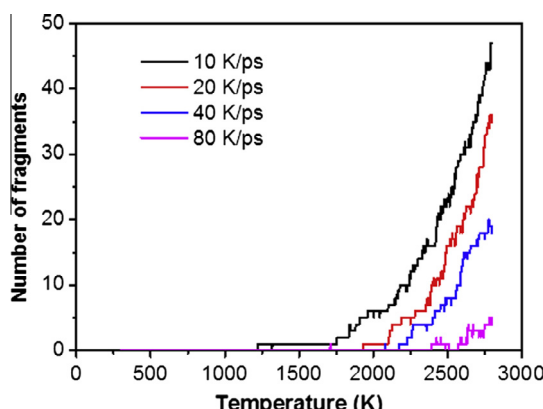


Fig. 2. Determination of initiation reactive temperature using NVT RMD at heating rates of 10, 20, 40 and 80 K/ps.

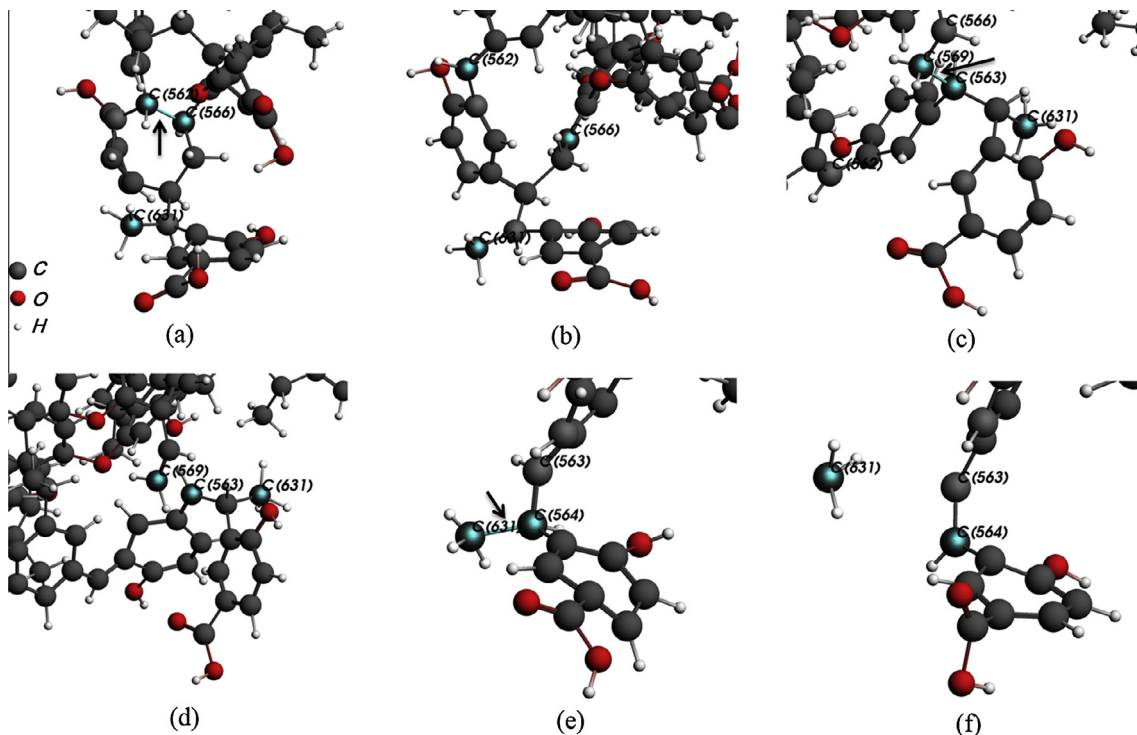


Fig. 3. Snapshots from ReaxFF heat up MD simulations show the initiation of reactions leading to methyl free radical with (a and b) and (c and d) for intra-molecular bond cleavages (C562–C566 and C569–C563), (e and f) for generation of methyl free radical. The arrows located the broken bonds.

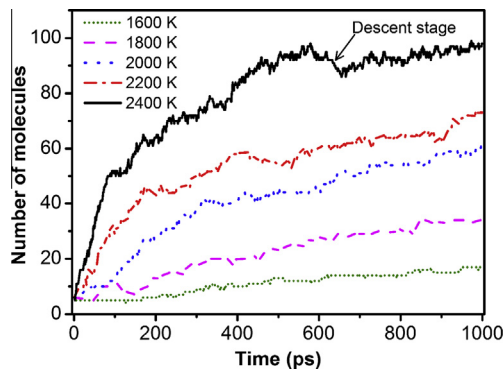


Fig. 4. Thermal decomposition of subbituminous coal model for NVT RMD simulations at 1600, 1800, 2000, 2200 and 2400 K.

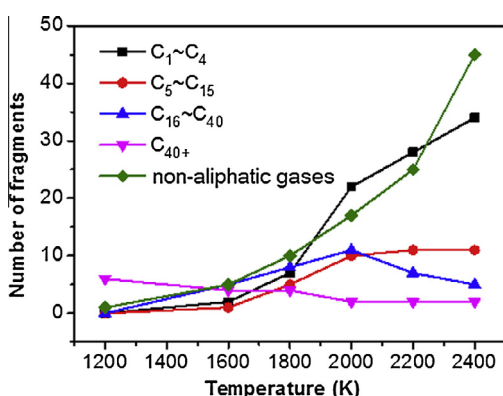


Fig. 5. Temperature evolution for products of different classes obtained by pyrolysis simulations using ReaxFF RMD at 1 ns.

on their average molecular weight around 80–500 amu. Those species of boiling points below 360 °C was considered as light tar [39], corresponding to the carbon number of C_5 – C_{15} compounds in this paper. The simulation results suggest that the pyrolysis temperature is an important factor to affect the product composition. Low temperature favors tar species generation while high temperature helps to produce small molecule fragments. Therefore, if we hope to produce tar by pyrolysis of subbituminous coal, the temperature of pyrolysis should be controlled in an appropriate range, not too low or too high.

For coal pyrolysis, it is commonly known that a higher heating rate has to cause the higher yields of pyrolysis oil and gas. This appears inconsistent with the clarification by MD simulations shown in Fig. 2. It in fact indicates that the fragments formed in heating up are not the final experimental pyrolysis products but the primary pyrolysis products. The former includes the effects of both free radical and secondary reactions. As one can see from Fig. 5, the generated products in MD simulations are majorly gas species below C_4 , while big-molecule species are not so many. This result shows that the MD simulations reproduce rather the characteristics of products without secondary reactions that are closely related to the field characteristics of flow, temperature and transfer in the reactor.

Typical gas products formed after 1 ns ReaxFF RMD simulations of subbituminous coal pyrolysis under various temperature conditions were shown in Fig. 6. Carbon dioxide was formed at low temperature, whose number increased firstly with temperature and then fluctuated in a small range (~10). This is due to that CO_2 is mainly derived from carboxyl groups whose number is a constant for this system. Many H_2O and CO were generated with rising temperature, especially when the temperature exceeded 2000 K. Hydrogen was observed in the RMD simulations at high temperatures. The number of CH_4 also increased with raising temperature, and then fluctuated at high temperatures. It implies that CH_4 is unstable and easy to react with other fragments at high temperatures. The

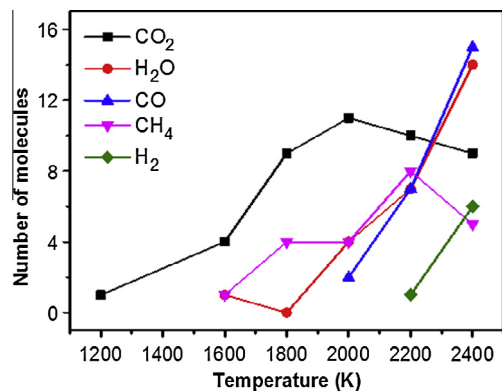


Fig. 6. Typical gas products generated after 1 ns ReaxFF MD simulations for subbituminous coal pyrolysis under various temperature conditions.

trend in the formation of these five typical gases with the variation of temperature is consistent with the experimental results [7,13]. These simulated results for these gases at 1800–2400 K was comparable with the experimental results for a subbituminous coal at 873–1273 K [39].

3.2. Major product species analysis

The temperature effect of the chemical composition is shown in Table 1, which is observed after the 1 ns NVT simulations of Hatcher's model at 1600, 1800, 2000 and 2200 K, respectively. The decomposition products are divided into five classes of compounds, involving small molecular C₄₋ compounds, light tar C₅₋₁₅ compounds, heavy tar C₁₆₋₄₀ compounds, large molecular C₄₀₊ char and non-aliphatic gases. The results show that the number of low molecular weight species (C₁₅₋ compounds) increased with the increase of simulation temperatures. However, at high temperatures (2000 and 2200 K), the large molecular weight species (C₁₆₊ compounds) decreased comparing with those at low temperatures, indicating that large molecular species decomposed into small molecular species at high temperatures.

For non-aliphatic and C₄₋ compounds, two representative species are CO₂ and CH₄. The number of CO₂ formation is about 10, which is stable at high temperatures. There are many C₄₋ species observed at the end of the RMD simulation with the temperature 2000 K. More interestingly, C₉H₉O is unique fragment for C₅₋₁₅ compounds after 1 ns RMD simulation with temperatures at 1600 and 1800 K, suggesting that the C₉H₉O group is liable to leave from the macromolecule. However, C₉H₉O is not stable at high temperatures, for example at 2000 K, which can either bind a hydrogen atom to form C₉H₁₀O or react with another group to produce a large fragment. The number of heavy tar composition of C₁₆₋₄₀ compounds increased from 1600 to 2000 K while decreasing at 2200 K, which means that this kind of compounds may either decompose into smaller fragments or aggregate with other fragments to form larger fragments. The C₄₀₊ compounds decomposed into non-aliphatic gases and tars. The weight for C₄₀₊ compounds at 2200 K is greater than that at 2000 K, indicating that these compounds at 2200 K may be formed by intermolecular polymerization.

In order to further study the evolution of species during the pyrolysis process, the changes of decomposed compounds over simulation times were analyzed for 1 ns NVT RMD simulation at 2000 K, as shown in Table 2. The number of small fragments (non-aliphatic, C₄₋ and C₅₋₁₆ compounds) increased with prolonging simulation time, while the fluctuations for the carbon content of C₁₆₋₄₀ compounds occur during last 600 ps. These mean that

Table 1

Chemical molecules observed after 1 ns NVT simulation at 1600, 1800, 2000 and 2200 K for Hatcher model.

1600 K	1800 K	2000 K	2200 K
<i>Non-aliphatic gases</i>			
4 CO ₂	9 CO ₂	11 CO ₂	10 CO ₂
1 H ₂ O	1 H ₂	2 CO	7 CO
		4 H ₂ O	7 H ₂ O
		1 H ₂	
<i>C₄₋ compounds</i>			
1 CH ₄	1 CH ₃	1 CH ₃	1 CH ₃
1 C ₂ H ₄	4 CH ₄	4 CH ₄	8 CH ₄
	1 C ₂ H ₄ O	2 C ₂ H ₂	3 C ₂ H ₂
	1 C ₂ H ₄	4 C ₂ H ₄	1 C ₂ H ₃
		1 C ₂ H ₅	4 C ₂ H ₄
		1 CH ₄ O	1 CH ₂ O
		4 C ₂ H ₂ O	1 CH ₄ O
		2 C ₃ H ₆	2 C ₂ H ₂ O
		2 C ₄ H ₄	4 C ₃ H ₆
		1 C ₄ H ₄ O	1 C ₃ H ₂ O
			2 C ₄ H ₄ O
<i>C₅₋₁₅ compounds</i>			
1 C ₉ H ₉ O	5 C ₉ H ₉ O	1 C ₆ H ₆	2 C ₅ H ₅
		1 C ₈ H ₆ O	1 C ₆ H ₅ O
		1 C ₁₀ H ₁₀	1 C ₉ H ₇
		2 C ₉ H ₁₀ O	1 C ₈ H ₇ O
		1 C ₁₀ H ₁₀ O	1 C ₉ H ₆ O
		1 C ₁₂ H ₁₀	1 C ₁₀ H ₁₀ O ₂
		1 C ₁₂ H ₁₃ O	1 C ₁₁ H ₁₄ O
		1 C ₁₅ H ₁₄ O	1 C ₁₃ H ₁₂
		1 C ₁₅ H ₁₁ O ₂	1 C ₁₄ H ₁₁ O
			1 C ₁₅ H ₁₂ O ₂
<i>C₁₆₋₄₀ compounds</i>			
1 C ₂₄ H ₂₂ O ₃	1 C ₁₇ H ₁₃ O ₃	1 C ₁₆ H ₁₂ O ₃	1 C ₁₇ H ₁₃ O ₂
1 C ₂₅ H ₂₀ O ₅	1 C ₂₀ H ₂₁ O	1 C ₁₉ H ₁₅ O	1 C ₁₇ H ₁₄ O ₃
1 C ₂₆ H ₂₄ O ₄	1 C ₂₂ H ₁₇ O ₃	1 C ₁₉ H ₁₄ O ₂	1 C ₁₉ H ₁₄ O ₃
1 C ₂₅ H ₂₃ O ₅	1 C ₂₃ H ₁₉ O ₃	1 C ₁₉ H ₁₅ O ₃	1 C ₂₅ H ₂₄ O ₃
1 C ₃₀ H ₃₂ O ₄	1 C ₂₅ H ₂₂ O ₂	2 C ₂₀ H ₂₂ O ₃	1 C ₃₄ H ₂₅
	1 C ₂₅ H ₂₁ O ₅	1 C ₂₃ H ₂₀ O	1 C ₃₂ H ₂₅ O ₃
	1 C ₃₄ H ₃₀ O ₄	1 C ₂₅ H ₁₇ O ₂	1 C ₄₀ H ₃₃ O ₆
	1 C ₃₄ H ₃₁ O ₄	1 C ₂₅ H ₂₁ O ₂	
		1 C ₃₅ H ₂₇ O ₄	
		1 C ₃₉ H ₂₈ O ₄	
<i>C₄₀₊ compounds</i>			
1 C ₆₀ H ₅₄ O ₁₀	1 C ₄₃ H ₃₇ O ₅	1 C ₄₇ H ₃₉ O ₆	1 C ₈₄ H ₆₄ O ₆
1 C ₈₇ H ₈₂ O ₁₀	1 C ₅₃ H ₄₉ O ₆	1 C ₆₂ H ₅₂ O ₈	1 C ₉₀ H ₆₆ O ₈
1 C ₁₁₇ H ₁₀₆ O ₁₈	1 C ₈₅ H ₇₅ O ₁₁		
1 C ₁₂₄ H ₁₁₀ O ₁₅	1 C ₉₁ H ₈₃ O ₁₁		

many small fragments came from the decomposition of C₁₆₋₄₀ compounds. Most of the fragments C₁₆–C₄₀ was unique due to the limitation of system scale, except for the fragments C₂₀H₂₂O₃ in Table 2, whose number increased to 2 at 1 ns, including two isomers with the same phenol skeleton and different substituent group at 2-position of phenol, as shown in [supplementary material](#). Due to the limitation of simulation time, we did not observe further variation of the fragment C₂₀H₂₂O₃, which may be decomposed to form phenolic products if increasing the simulation time. The weight for C₄₀₊ compounds at 1000 ps is greater than that at 600 ps, indicating that there are polymerizations to occur among different compounds. At the beginning stage of RMD simulation, more changes occurred between macromolecules and only three kinds of small molecular fragments were produced at 100 ps, including CO₂, CH₃ and C₉H₉O. The free radical CH₃ was formed at the beginning of MD simulation, which is a precursor for producing CH₄. Although there was no H₂ observed at the end of 1 ns RMD simulation, it would still be present in the middle stage of this simulation. We focused on the evolution of five compounds including CO₂, CO CH₄, H₂ and C₉H₉O, and the time courses of the number of them are shown in Fig. 7.

Table 2

Chemical molecules observed with 1 ns of NVT simulation at 2000 K for Hatcher model.

100 ps	400 ps	600 ps	1000 ps
<i>Non-aliphatic gases</i>			
2 CO ₂	7 CO ₂	9 CO ₂	11 CO ₂
3 H ₂ O	2 H ₂ O	4 H ₂ O	
1 CO	1 CO	2 CO	
1 H ₂	1 H ₂		
<i>C₄– compounds</i>			
1 CH ₃	2 CH ₄	2 CH ₄	1 CH ₃
2 C ₂ H ₄	1 C ₂ H ₂	4 C ₂ H ₄	
1 C ₃ H ₆ O	2 C ₂ H ₄	2 C ₂ H ₂	
1 C ₂ H ₂ O	1 CH ₃ O	4 C ₂ H ₄	
1 C ₄ H ₄ O	3 C ₂ H ₂ O	1 C ₂ H ₅	
	1 C ₄ H ₃	1 CH ₄ O	
	1 C ₄ H ₄ O	4 C ₂ H ₂ O	
		2 C ₃ H ₆	
		2 C ₄ H ₄	
		1 C ₄ H ₄ O	
<i>C₅–₁₅ compounds</i>			
1 C ₉ H ₉ O	1 C ₆ H ₈	1 C ₆ H ₇	1 C ₆ H ₆
1 C ₈ H ₆ O	1 C ₈ H ₆ O	1 C ₈ H ₆ O	1 C ₈ H ₆ O
3 C ₉ H ₉ O	2 C ₉ H ₁₀ O	2 C ₉ H ₁₀	1 C ₁₀ H ₁₀
1 C ₁₀ H ₁₀	1 C ₁₀ H ₁₀	2 C ₉ H ₁₀ O	2 C ₉ H ₁₀ O
1 C ₁₀ H ₁₀ O	1 C ₁₀ H ₁₀ O	1 C ₁₀ H ₁₀ O	1 C ₁₀ H ₁₀ O
1 C ₁₅ H ₁₃ O	1 C ₁₁ H ₁₀ O	1 C ₁₁ H ₁₀ O	1 C ₁₂ H ₁₀
	1 C ₁₅ H ₁₃ O	1 C ₁₅ H ₁₃ O	1 C ₁₂ H ₁₃ O
			1 C ₁₅ H ₁₄ O
			1 C ₁₅ H ₁₁ O ₂
<i>C₁₆–₄₀ compounds</i>			
1 C ₁₈ H ₁₆ O ₂	1 C ₁₆ H ₁₅ O ₂	1 C ₁₆ H ₁₄ O ₂	1 C ₁₆ H ₁₂ O ₃
1 C ₂₅ H ₂₁ O ₅	1 C ₁₉ H ₁₄ O ₂	1 C ₁₉ H ₁₄ O ₂	1 C ₁₉ H ₁₅ O
1 C ₂₅ H ₂₃ O ₅	1 C ₂₀ H ₁₆ O ₃	1 C ₂₀ H ₂₁ O ₃	1 C ₁₉ H ₁₄ O ₂
1 C ₃₉ H ₃₉ O ₅	1 C ₂₀ H ₂₁ O ₃	1 C ₂₀ H ₂₂ O ₃	1 C ₁₉ H ₁₅ O ₃
	1 C ₂₀ H ₂₂ O ₃	1 C ₂₃ H ₁₈ O ₃	2 C ₂₀ H ₂₂ O ₃
	1 C ₂₅ H ₂₁ O ₂	1 C ₂₅ H ₂₁ O ₂	1 C ₂₃ H ₂₀ O
	1 C ₂₄ H ₂₀ O ₅	1 C ₂₉ H ₂₈ O ₃	1 C ₂₅ H ₁₇ O ₂
	1 C ₂₆ H ₂₃ O ₄	1 C ₃₅ H ₃₀ O ₄	1 C ₂₅ H ₂₁ O ₂
	1 C ₂₉ H ₂₈ O ₃	1 C ₄₀ H ₃₈ O ₅	1 C ₃₅ H ₂₇ O ₄
	1 C ₃₀ H ₂₇ O ₄		1 C ₃₉ H ₂₈ O ₄
	1 C ₃₄ H ₂₆ O ₃		
<i>C₄₀₊ compounds</i>			
1 C ₄₁ H ₃₆ O ₈	1 C ₅₃ H ₄₇ O ₆	1 C ₄₁ H ₃₀ O ₅	1 C ₄₇ H ₃₉ O ₆
1 C ₆₄ H ₅₉ O ₉	1 C ₅₇ H ₅₁ O ₆	1 C ₄₁ H ₄₁ O ₅	1 C ₆₂ H ₅₂ O ₈
1 C ₆₄ H ₆₁ O ₉	1 C ₆₄ H ₅₃ O ₁₁	1 C ₅₁ H ₄₆ O ₅	
1 C ₇₁ H ₆₇ O ₁₂			
1 C ₈₇ H ₇₉ O ₁₂			
1 C ₈₈ H ₇₉ O ₁₂			

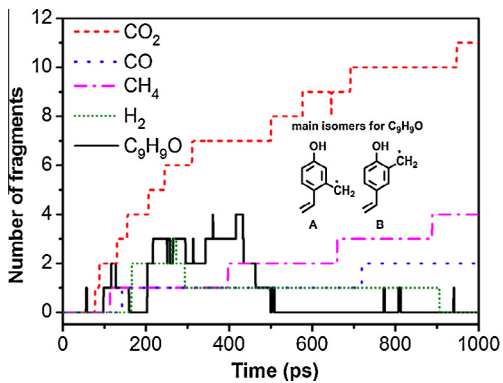


Fig. 7. Analyses of typical species in ReaxFF MD simulations of initial stage for subbituminous coal pyrolysis at 2000 K.

As shown in the figure, the number of CO₂ increased rapidly before 400 ps and tended to be stable at about 10 after 600 ps. Two CO molecules were formed at 140 and 720 ps. The number

of CH₄ increased with time and stabilized to 4 at last. There were three H₂ formed during the RMD simulation, but they were very active in this system and all disappeared at 1000 ps. The fragment C₉H₉O was formed before 400 ps and then reacts with other free radical to produce large or small compounds. Two dominant isomers for C₉H₉O appearing during RMD simulations at 1800 and 2000 K are shown in Fig. 7, which will be discussed in the following text.

3.3. Formation mechanisms of typical gas and liquid products

The formation of carbon oxides (CO and CO₂) is mainly derived from the dissociation and emission of oxygenated functional groups in the pyrolysis process of subbituminous coal. Previous simulation results have proven that direct decarboxylation contributes to the formation of CO₂ in both pyrolysis and oxidation processes [29,31]. This formation process of CO₂ was also observed in our simulations. For the simulation at 2000 K, hydrogen of the carboxyl groups firstly transferred to hydrogen acceptors that were derived from four types of oxygen-containing groups: ketone, phenoxy radicals, enol radicals and alkynol radicals, as shown in Fig. 8a. Then 11 CO₂ molecules would be formed by decarboxylation of carboxyl free radicals. However, Behar and Hatcher [51] reported that the increase in CO₂ did not derive entirely from loss of carboxyl carbon, which also came from loss of carbonyl carbon in NMR spectra. Thus, loss of carbonyl carbon may be firstly to form the precursor of CO₂, for example CO, as can be seen in our simulations. Comparing with the scales of experimental time and temperature, the RMD simulation is just suitable for studying the initial process of coal pyrolysis.

Two formation pathways of CO derived from different oxygenated functional groups were observed in our RMD simulations, which were shown in Figs. 9 and 10, respectively. In pathway 1, CO derived from the carbonyl group was formed by the cleavage of C_{al}—CO bond, following the cleavage of C_{ar}—CO bond, as shown in Fig. 9. The order of bond cleavages accords with the rule of minimal energy bond breaking firstly. The bond energies for the breaking C_{al}—CO and C_{ar}—CO bonds, using a model compound, were calculated through DFT method with the basis set superposition error (BSSE) correction. The bond energy for C_{ar}—CO is higher than that for C_{al}—CO bond (94.93 vs 77.94 kcal/mol).

The formation pathway 2 of CO derived from the carboxyl group is illustrated in Fig. 10. The carboxyl group extracted a hydrogen atom from the hydrogen donor to form —C(OH)₂ free radical group (Fig. 10b). Then the ether linkage broke down to form C_{ar}—O· free radical, which is a strong hydrogen acceptor and obtained a hydrogen from a hydroxyl group, as shown in Fig. 10c–e. The unstable —C(OH)₂ free radical group lost a hydrogen atom to recover the carboxyl group (Fig. 10f). Next, a methyl free radical attacked the carboxyl group to form methanol (Fig. 10g and h), which is a crucial step in the formation of CO derived from the carboxyl group. Finally, cleavage of C_{ar}—C bond to produce CO. The results for these two pathways indicate that the formation of CO may be originated from different oxygenated functional groups and go through a series of complex processes, such as C—C bond cleavages, intermolecular hydrogen transfers, the ether bond cleavage and the dehydroxylation of the carboxyl group.

The primary components of pyrolysis gas contain methane and hydrogen, whose formation reactions were shown in Fig. 8b and c. Three quarters of CH₄ molecules were produced by CH₃ free radical abstracting hydrogen atom from the phenolic hydroxyl group and one CH₄ molecule was formed by hydrogen transfer from the alkyl group to CH₃. Hydrogen was generated by three ways: (1) in a common fragment, two hydrogen atoms of methyl directly leave; (2) two hydrogen atoms are derived from —CH₂— and —CH₃ groups in different fragments; (3) hydroxyl hydrogen bound with the

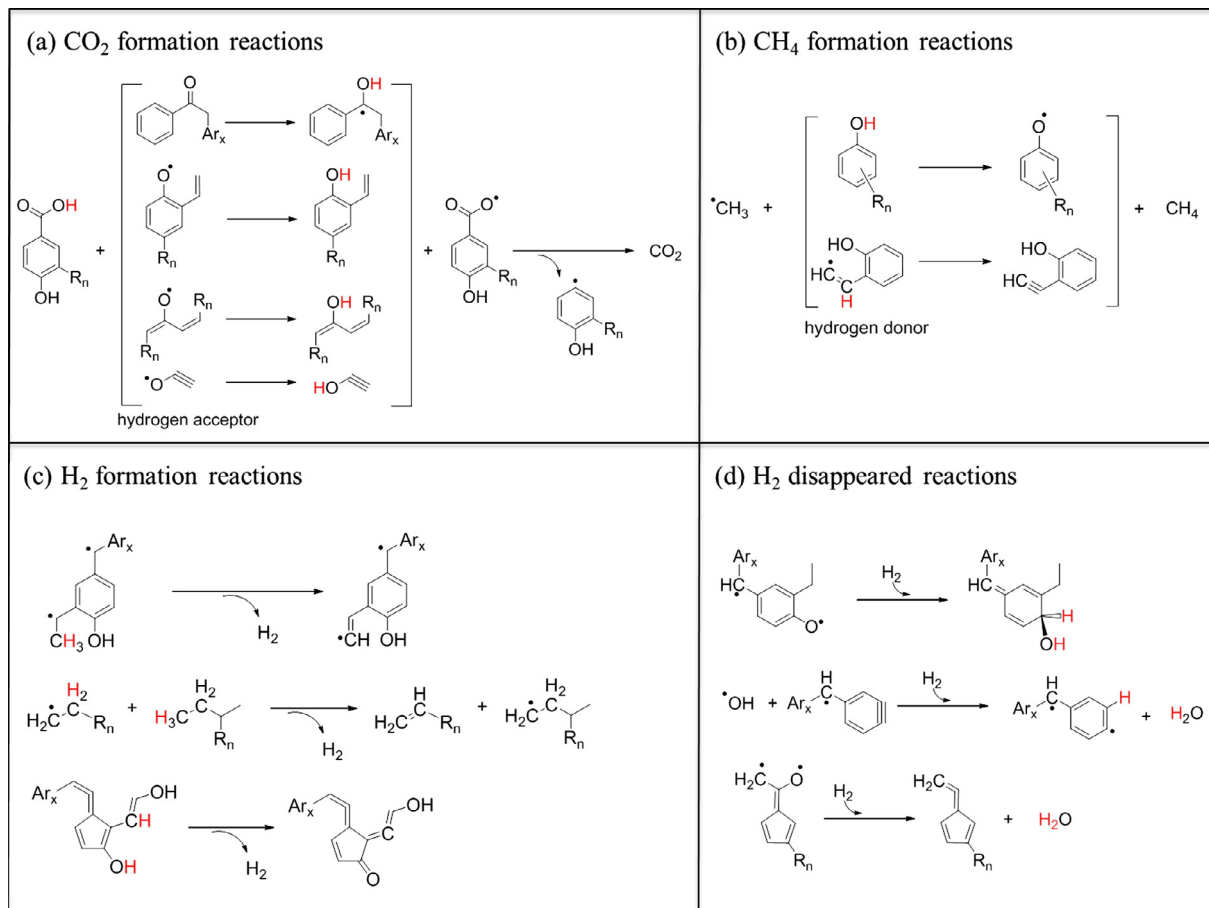


Fig. 8. Examples of chemical reactions for typical gases during RMD at 2000 K: (a–c) formation pathways of CO_2 , CH_4 and H_2 and (d) disappear reactions of H_2 . (R_n : aliphatic group; Ar_x : aromatic group).

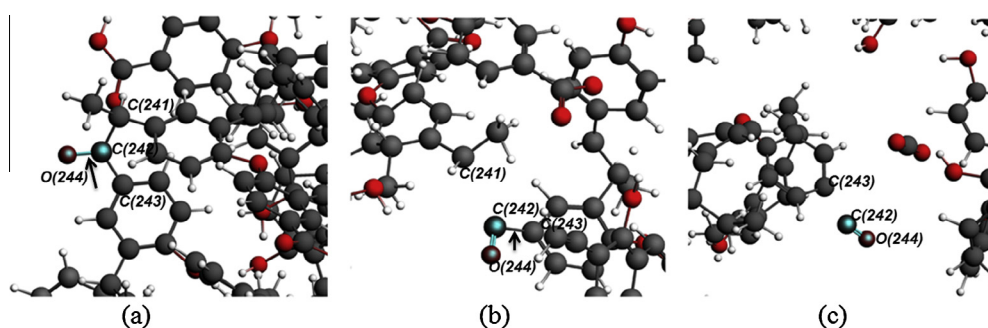


Fig. 9. The formation pathway 1 of CO derived from the carbonyl group. (a) For the intact carbonyl group, (b) for the bond C241–C242 breaking and (c) for the cleavage of bond C242–C243 and generation of CO. The arrows located the broken bonds.

hydrogen atom on vinyl to form H_2 and then the electron rearrangement occurred to increase the conjugated double bonds in the residual structure. As can be seen from Fig. 7, H_2 was formed during the middle stage of RMD simulation at 2000 K, but it disappeared after 1 ns RMD. Thus, we have tracked the reactions with hydrogen participation. Fig. 8d shows us that H_2 reacted with oxygen-containing free radicals to stabilize them and form hydroxyl or H_2O , which suggests that H_2 was of high reactivity in this system. During the formation pathway of gas product, phenolic hydroxyl groups play an important role in hydrogen transfer, as a good hydrogen-donor, which can provide H^+ for the formation of CH_4 or H_2 . While a phenolic hydroxyl group loses H^+ to become a phenoxyl radical, it can abstract hydrogen again from the carboxyl or

other hydrogen-donor in the vicinity, such as the second type of CO_2 formation reactions (Fig. 8a). In addition, small molecules or radicals have a superior mobility, which also increases the chance of collision with other active fragments, thereby improving their reactivity.

Light tar is the desired component formed during coal pyrolysis. The fragment $\text{C}_9\text{H}_9\text{O}$ is a pivotal species during the RMD simulations of pyrolysis process for Hatcher subbituminous coal. We observed that there were several isomers for $\text{C}_9\text{H}_9\text{O}^\cdot$ free radical during all RMD simulations. The formation pathways of two dominant isomers were studied, which may be the precursor of cresol under appropriate conditions. The formation pathway for the isomer A of $\text{C}_9\text{H}_9\text{O}^\cdot$ fragment was shown in Fig. 11. The initial structure

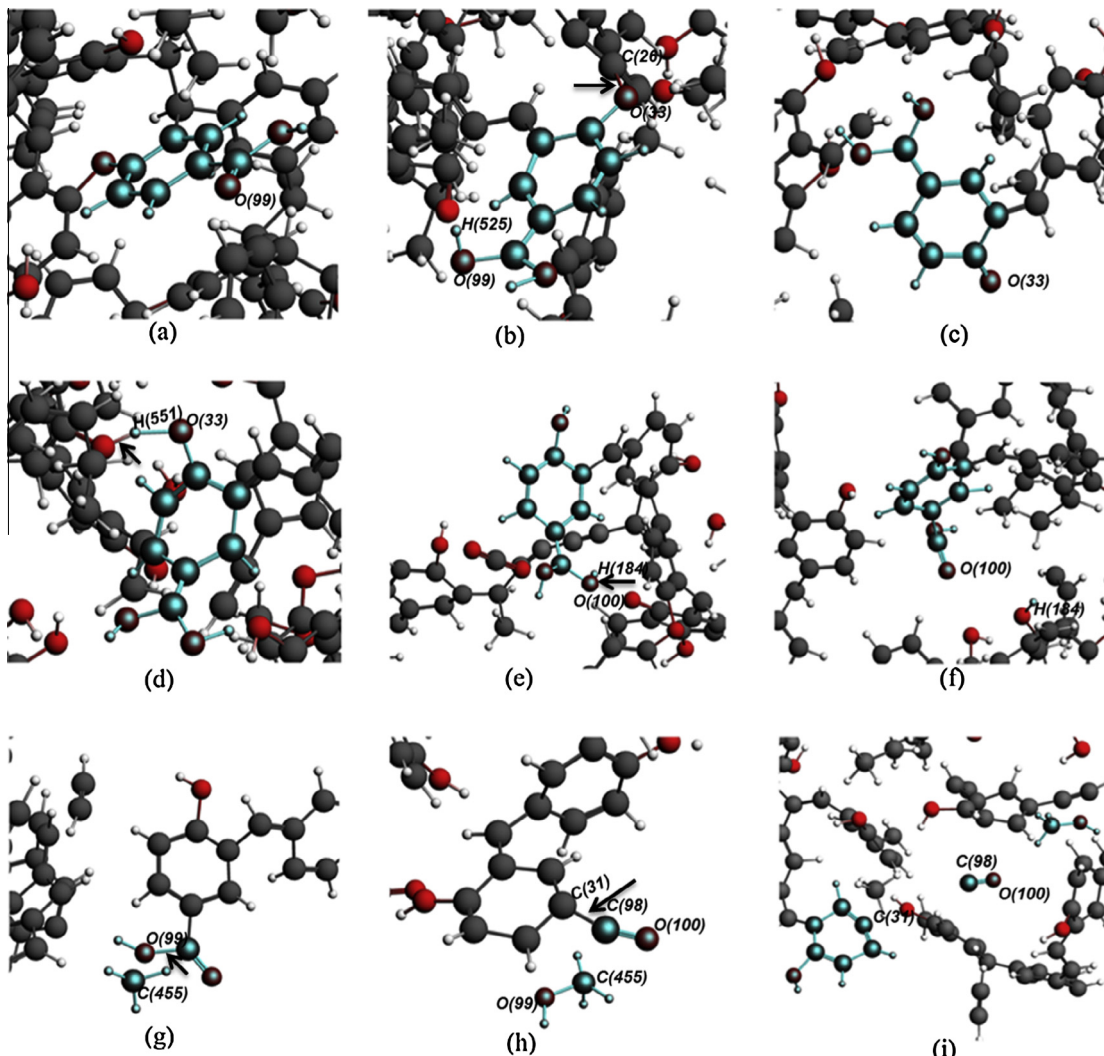


Fig. 10. The formation pathway 2 of CO derived from the carboxyl group. (a–c) for the formation of O99–H525 bond and the cleavage of ether bond C26–O33, (d) for the transition state of H551 from a hydroxyl group to O33, (e and f) for the cleavage of bond O100–H184 and H184 binding with an oxygen radical, (g and h) for the hydroxyl leaving from the carboxyl group and the formation of methanol, and (i) for the formation of CO. The arrows located the broken bonds.

firstly went through ring rearrangement to make one of the two six-member rings change to the five-member ring (Fig. 11a–c). Then the C271–C273 bond broke down to form a fragment containing double rings with a free electron at C273 (Fig. 11d and e). Finally, electron rearrangements occur among the atoms of C273, C280 and C282, leading to the cleavage of C280–C282 bond to form the C273=C280 double bond and a free radical at C282 (Fig. 11f).

Cresol is an important component of tar produced from subbituminous coal pyrolysis [52,53]. Thus, as a precursor of cresol, the formation pathway for the isomer B of C_9H_9O fragment was investigated by combining ReaxFF MD simulations with DFT calculations. As can be seen from Fig. 12, the radical C_9H_9O with 2,4-position cyclization (R0) was observed to be formed at the initial stage of the ReaxFF MD trajectories, which went through a ring-opening transition state to produce the isomer (IM1) of C_9H_9O fragment. Then isomerization will occur from IM1 to the isomer B (IM2) by a smooth transition state (TS2) of dihedral twist. If there are active hydrogen atoms near the reaction site in this system, IM2 can abstract hydrogen atom to saturate the 2-position methylene radical. The active hydrogen atoms may involve hydrogen free radical or other groups to easily lose a hydrogen atom. The isomer B of C_9H_9O can bond with a hydrogen free radical existing near the reaction site to form a stable intermediate P0, as shown in

Fig. 12. The energy of the transition state is 187.5 kcal/mol based on that of $C_9H_{10}O$, calculated by DFT methods. The P0 is one of C3 phenols, in accordance with the experimental data of subbituminous coal pyrolysis from Hatcher [19,40] and others [52,54]. Because the pyrolysis process could provide sufficient energy, the 4-vinyl group of intermediate $C_9H_{10}O$ (P0) may interact with 5-carbon in aromatic ring to form intermediate (IM3) via a transition state TS3. If there are H_2 in the system, one of double bonds in IM3 can be saturated via TS4 to form a low-energy intermediate IM4. Although the energy for TS4 is up to 114.2 kcal/mol, it is still lower than that for the reactant C_9H_9O (R0), which has been observed in ReaxFF MD simulations. Finally the intermediate IM4 can decompose into *o*-cresol and ethylene via TS5. The energy for products is −4.6 kcal/mol, lower than that of $C_9H_{10}O$, which is a favorable process in energy. DFT calculations only demonstrated one of probable formation pathways for cresol, but it was a valuable approach for understanding the formation mechanisms of typical products.

This work mainly focused on the formation process of typical gas and liquid products during pyrolysis. For the NVT simulations at different temperatures, we thought that the reactions for the generation of pyrolysis gas and liquid products can be extrapolated to lower temperatures. The scale of the simulation system is much less than that for the coal particle, so the reactions for large

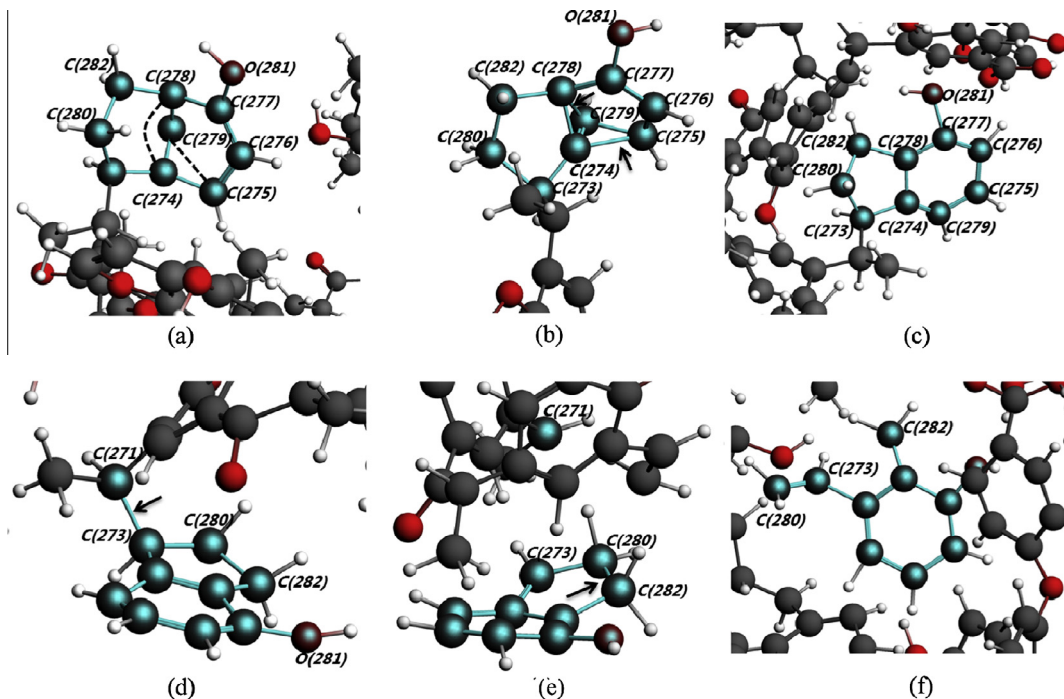


Fig. 11. The formation pathway for isomer A observed during RMD simulation at 2000 K. Snapshots (a–c) show the arrangement of double six-member rings, including the bond formations (C278–C274 and C279–C275) and cleavages (C278–C279 and C174–C275). Snapshots (d and e) show the formation of isomer A by the bond cleavages (C271–C273 and C280–C282). The dashed lines indicated the bond formation and the arrows located the bond breaking.

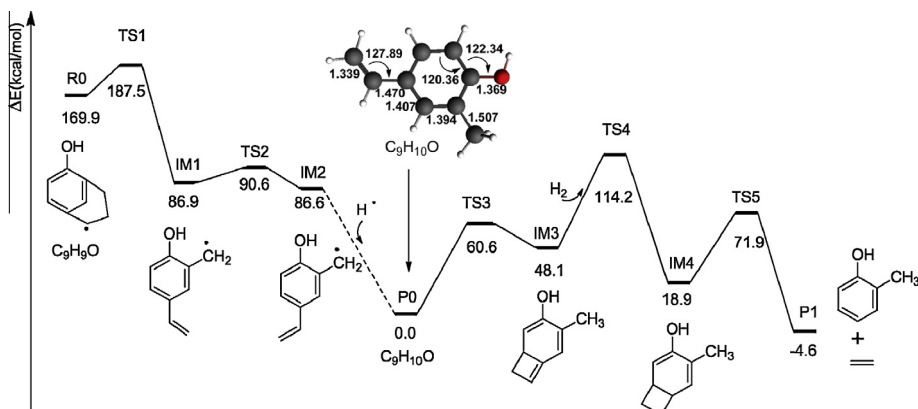


Fig. 12. Energy diagrams of $\text{C}_9\text{H}_{10}\text{O}$ formation and its reaction pathway in the presence of H_2 .

fragments (char) cannot be extrapolated to lower temperatures. At high temperatures, the large fragments are liable to be pyrolyzed to form small fragments. Further simulations will be conducted to compare the formation mechanisms of the same products in different coal structures. In addition, the simulation system is not involved heteroatoms S and N that are often reactive in pyrolysis of most coals, which will be the target of future studies.

4. Conclusion

In this article, we have investigated the pyrolysis mechanisms of subbituminous coal using the ReaxFF reactive molecular dynamics simulations assisted by DFT calculations. The results demonstrate that the thermal decomposition is initiated by C–C bond cleavage following intramolecular hydrogen transfer. During 1 ns reactive molecular dynamics simulations, there are many fragments to be observed, including small molecule gases, precursors of phenols and other species of tar. With increasing temperature

and simulation time, the second polymerizations appeared among different radical fragments. The initial pathway for the formation of CO is through the decarbonylation of carbonyl or carboxyl groups. Phenoxy groups can provide hydrogen as hydrogen donor and lose H^+ to become hydrogen acceptor, which play a key role in the formation pathway of CO_2 , CH_4 and H_2 . The free radicals of $\text{C}_9\text{H}_{9}\text{O}^\cdot$ are observed to be an important fragment, as the precursor of cresol and C3 phenol, which can capture hydrogen radical to form a relatively stable intermediate $\text{C}_9\text{H}_{10}\text{O}$ and then continue to produce o-cresol and ethylene in the presence of hydrogen resource. The information on mechanisms and chemical events during the pyrolysis processes of Hather subbituminous coal model is coincident with the results of previous experiments. These results of the study validated that the approach of ReaxFF MD simulation combined with DFT calculation can provide useful insights into complicated reaction processes and give a reasonable atomistic description of the initial pyrolysis mechanisms for subbituminous coal.

Acknowledgments

This work was financially supported by the National Natural Science Foundation of China (21306210), the National Basic Research Program of China (2011CB201304), the International Science & Technology Cooperation Program of China (2013DFG60060) and the Strategic Priority Research Program of Chinese Academy of Sciences (XDA07010100).

Appendix A. Supplementary material

Supplementary data associated with this article can be found, in the online version, at <http://dx.doi.org/10.1016/j.fuel.2014.06.005>.

References

- [1] Subbituminous coal. In: encyclopaedia britannica. <<http://www.britannica.com/EBchecked/topic/570576/subbituminous-coal>>; 2013.
- [2] Borah RC, Ghosh P, Rao PG. A review on devolatilization of coal in fluidized bed. *Int J Energy Res* 2011;35:929–63.
- [3] Solomon PR, Fletcher TH, Pugmire RJ. Progress in coal pyrolysis. *Fuel* 1993;72:587–97.
- [4] Vandebroucke M, Largeau C. Kerogen origin, evolution and structure. *Org Geochem* 2007;38:719–833.
- [5] van Heek KH, Hodek W. Structure and pyrolysis behavior of different coals and relevant model substances. *Fuel* 1994;73:886–96.
- [6] Wilkins RWT, George SC. Coal as a source rock for oil: a review. *Int J Coal Geol* 2002;50:317–61.
- [7] Solomon PR, Serio MA, Suuberg EM. Coal pyrolysis: experiments, kinetic rates and mechanisms. *Prog Energy Combust Sci* 1992;18:133–220.
- [8] Morgan TJ, Kandiyoti R. Pyrolysis of coals and biomass: analysis of thermal breakdown and its products. *Chem Rev* 2014;114:1547–607.
- [9] Mathews JP, Chaffee AL. The molecular representations of coal – a review. *Fuel* 2012;96:1–14.
- [10] Tromp PJJ, Moulijn J. Slow and rapid pyrolysis of coal. In: Yürüm Y, editors. New trends in coal science, vol. 244, Netherlands: Springer; 1988. p. 305–38.
- [11] Deshpande GV, Solomon PR, Serio MA. Crosslinking reactions in coal pyrolysis. *Am Chem Soc Div Fuel Chem Prep* 1988;33:310–21.
- [12] Solomon PR, Hamblen DG, Carangelo RM, Serio MA, Deshpande GV. General model of coal devolatilization. *Energy Fuels* 1988;2:405–22.
- [13] Serio MA, Hamblen DG, Markham JR, Solomon PR. Kinetics of volatile product evolution in coal pyrolysis: experiment and theory. *Energy Fuels* 1987;1:138–52.
- [14] Freihaut JD, Solomon PR, Seery DJ. In situ study of rapid coal pyrolysis using FTIR. *Abstr Pap Am Chem Soc* 1980;180:161–70.
- [15] Solomon PR, Carangelo RM. FT-i.r. analysis of coal: 2. Aliphatic and aromatic hydrogen concentration. *Fuel* 1988;67:949–59.
- [16] Fletcher TH, Kerstein AR, Pugmire RJ, Solum MS, Grant DM. Chemical percolation model for devolatilization.3. Direct use of ¹³C NMR data to predict effects of coal type. *Energy Fuels* 1992;6:414–31.
- [17] Solum MS, Pugmire RJ, Grant DM, Fletcher TH, Solomon PR. Solid-state ¹³C NMR studies of coal char structure evolution. *Am Chem Soc Div Fuel Chem Prep* 1989;34:1337–44.
- [18] Lievens C, Ci D, Bai Y, Ma L, Zhang R, Chen JY, et al. A study of slow pyrolysis of one low rank coal via pyrolysis GC/MS. *Fuel Process Technol* 2013;116:85–93.
- [19] Hatcher PG, Lerch HE, Kotra RK, Verheyen TV. Pyrolysis g.c.-m.s. of a series of degraded woods and coalified logs that increase in rank from peat to subbituminous coal. *Fuel* 1988;67:1069–75.
- [20] Huffman GP, Mitra S, Huggins FE, Shah N, Vaidya S, Lu FL. Quantitative-analysis of all major forms of sulfur in coal by X-ray absorption fine-structure spectroscopy. *Energy Fuels* 1991;5:574–81.
- [21] Sugawara K, Sugawara T, Shirai M. Sulfur behavior in rapid pyrolysis of coals with chemical pretreatments. *Jpn J Appl Phys* 1999;1(38):608–11.
- [22] Zhu Q, Money SL, Russell AE, Thomas KM. Determination of the fate of nitrogen functionality in carbonaceous materials during pyrolysis and combustion using X-ray absorption near edge structure spectroscopy. *Langmuir* 1997;13:2149–57.
- [23] Mullins OC, Mitra Kirkley S, Vanelp J, Cramer SP. Molecular-structure of nitrogen in coal from XANES spectroscopy. *Appl Spectrosc* 1993;47:1268–75.
- [24] Turner JA, Thomas KM, Russell AE. The identification of oxygen functional groups in carbonaceous materials by oxygen K-edge XANES. *Carbon* 1997;35:983–92.
- [25] van Duin ACT, Dasgupta S, Lorant F, Goddard WA. ReaxFF: a reactive force field for hydrocarbons. *J Phys Chem A* 2001;105:9396–409.
- [26] Chenoweth K, van Duin ACT, Dasgupta S, Goddard WA. Initiation mechanisms and kinetics of pyrolysis and combustion of JP-10 hydrocarbon jet fuel. *J Phys Chem A* 2009;113:1740–6.
- [27] Salmon E, van Duin ACT, Lorant F, Marquaire PM, Goddard WA. Thermal decomposition process in algaenan of *Botryococcus braunii* race L. Part 2: molecular dynamics simulations using the ReaxFF reactive force field. *Org Geochem* 2009;40:416–27.
- [28] Castro-Marcano F, Kamat AM, Russo MF, van Duin ACT, Mathews JP. Combustion of an Illinois No. 6 coal char simulated using an atomistic char representation and the ReaxFF reactive force field. *Combust Flame* 2012;159:1272–85.
- [29] Yan GC, Zhang ZQ, Yan KF. Reactive molecular dynamics simulations of the initial stage of brown coal oxidation at high temperatures. *Mol Phys* 2013;111:147–56.
- [30] Chen B, Diao Z-j, Lu H-y. Using the ReaxFF reactive force field for molecular dynamics simulations of the spontaneous combustion of lignite with the Hatcher lignite model. *Fuel* 2014;116:7–13.
- [31] Salmon E, van Duin ACT, Lorant F, Marquaire PM, Goddard WA. Early maturation processes in coal. Part 2: reactive dynamics simulations using the ReaxFF reactive force field on Morwell Brown coal structures. *Org Geochem* 2009;40:1195–209.
- [32] Chen B, Wei XY, Yang ZS, Liu C, Fan X, Qing Y, et al. ReaxFF reactive force field for molecular dynamics simulations of lignite depolymerization in supercritical methanol with lignite-related model compounds. *Energy Fuels* 2012;26:984–9.
- [33] Zhang JL, Weng XX, Han Y, Li W, Cheng JY, Gan ZX, et al. The effect of supercritical water on coal pyrolysis and hydrogen production: a combined ReaxFF and DFT study. *Fuel* 2013;108:682–90.
- [34] Zheng M, Li XX, Liu J, Guo L. Initial chemical reaction simulation of coal pyrolysis via reaxFF molecular dynamics. *Energy Fuels* 2013;27:2942–51.
- [35] Zheng M, Li XX, Liu J, Wang Z, Gong XM, Guo L, et al. Pyrolysis of Liulin coal simulated by GPU-based ReaxFF MD with cheminformatics analysis. *Energy Fuels* 2014;28:522–34.
- [36] Salmon E, Behar F, Lorant F, Hatcher PG, Marquaire PM. Early maturation processes in coal. Part 1: pyrolysis mass balance and structural evolution of coalified wood from the Morwell Brown Coal seam. *Org Geochem* 2009;40:500–9.
- [37] Wiser WH. Conversion of bituminous coal to liquids and gases: chemistry and representative processes. In: Petrakis L, Fraissard JP, editors. Magnetic resonance. Introduction, advanced topics and applications to fossil energy, vol. 124, Netherlands: Springer; 1984. p. 325–50.
- [38] Shinn JH. From coal to single-stage and two-stage products: a reactive model of coal structure. *Fuel* 1984;63:1187–96.
- [39] Zhang C, Wu RC, Xu GW. Coal pyrolysis for high-quality tar in a fixed-bed pyrolyzer enhanced with internals. *Energy Fuels* 2014;28:236–44.
- [40] Hatcher PG. Chemical structural models for coalified wood (vitrinite) in low rank coal. *Org Geochem* 1990;16:959–68.
- [41] Marvin was used for drawing, displaying and characterizing chemical structures, substructures and reactions, Marvin 5.12.4, ChemAxon. <http://www.chemaxon.com>; 2013.
- [42] Materials Studio, Version 4.0. Accelrys Software Inc, San Diego, CA; 2006.
- [43] Chenoweth K, van Duin ACT, Goddard WA. ReaxFF reactive force field for molecular dynamics simulations of hydrocarbon oxidation. *J Phys Chem A* 2008;112:1040–53.
- [44] van Duin ACT, Zeiri Y, Dubnikova F, Kosloff R, Goddard WA. Atomistic-scale simulations of the initial chemical events in the thermal initiation of triacetone triperoxide. *J Am Chem Soc* 2005;127:11053–62.
- [45] Mueller JE, van Duin ACT, Goddard WA. Application of the ReaxFF reactive force field to reactive dynamics of hydrocarbon chemisorption and decomposition. *J Phys Chem C* 2010;114:5675–85.
- [46] Baerends EJ, et al. ADF2013, SCM, Theoretical chemistry, Vrije Universiteit, Amsterdam, The Netherlands. <<http://www.scm.com>>; 2013.
- [47] Gaussian 03, Revision C02. Frisch M, Trucks G, Schlegel H, Scuseria G, Robb M, Cheeseman J, et al. Wallingford: Gaussian Inc.; 2004.
- [48] Becke AD. Density-functional thermochemistry. III. The role of exact exchange. *J Chem Phys* 1993;98:5648–52.
- [49] Lee CT, Yang WT, Parr RG. Development of the Colle-Salvetti correlation-energy formula into a functional of the electron-density. *Phys Rev B* 1988;37:785–9.
- [50] Nimz H. Beech lignin – proposal of a constitutional scheme. *Angew Chem Int Ed* 1974;13:313–21.
- [51] Behar F, Hatcher PG. Artificial coalification of a fossil wood from brown coal by confined system pyrolysis. *Energy Fuels* 1995;9:984–94.
- [52] Iglesias MJ, del Río JC, Laggoun-Défarge F, Cuesta MJ, Suárez-Ruiz I. Control of the chemical structure of perhydrous coals; FTIR and Py-GC/MS investigation. *J Anal Appl Pyrol* 2002;62:1–34.
- [53] Meuzelaar HLC, Harper AM, Hill GR, Given PH. Characterization and classification of Rocky-Mountain coals by Curie-Point pyrolysis mass-spectrometry. *Fuel* 1984;63:640–52.
- [54] Jiménez A, Iglesias MJ, Laggoun-Defarge F, Suárez-Ruiz I. Effect of the increase in temperature on the evolution of the physical and chemical structure of vitrinite. *J Anal Appl Pyrol* 1999;50:117–48.